Fish-inspired segment models for undulatory steady swimming

Bioinspiration & Biomimetics

OPEN ACCESS

PAPER

Fish-inspired segment models for undulatory steady swimming

Otar Akanyeti[1,*], Valentina Di Santo[2], Elsa Goerig[3,4], Dylan K Wainwright[5], James C Liao[6], Theodore Castro-Santos[4] and George V Lauder[3]

[1] Department of Computer Science, Aberystwyth University, Ceredigion, SY23 3FL, United Kingdom
[2] Division of Functional Morphology, Department of Zoology, Stockholm University, Stockholm, Sweden
[3] Museum of Comparative Zoology, Harvard University, Cambridge, MA, United States of America
[4] S.O. Conte Anadromous Fish Research Center, USGS, Turners Falls, MA, United States of America
[5] Department of Ecology and Evolutionary Biology, Yale University, New Haven, CT, United States of America
[6] Department of Biology, The Whitney Laboratory for Marine Bioscience, University of Florida, St. Augustine, FL, United States of America
* Author to whom any correspondence should be addressed.

E-mail: ota1@aber.ac.uk

RECEIVED
18 January 2022

REVISED
7 April 2022

ACCEPTED FOR PUBLICATION
29 April 2022

PUBLISHED
24 May 2022

Keywords: undulatory swimming, midline kinematics, multi-segment models, fish robots

Supplementary material for this article is available online

Abstract

Many aquatic animals swim by undulatory body movements and understanding the diversity of these movements could unlock the potential for designing better underwater robots. Here, we analyzed the steady swimming kinematics of a diverse group of fish species to investigate whether their undulatory movements can be represented using a series of interconnected multi-segment models, and if so, to identify the key factors driving the segment configuration of the models. Our results show that the steady swimming kinematics of fishes can be described successfully using parsimonious models, 83% of which had fewer than five segments. In these models, the anterior segments were significantly longer than the posterior segments, and there was a direct link between segment configuration and swimming kinematics, body shape, and Reynolds number. The models representing eel-like fishes with elongated bodies and fishes swimming at high Reynolds numbers had more segments and less segment length variability along the body than the models representing other fishes. These fishes recruited their anterior bodies to a greater extent, initiating the undulatory wave more anteriorly. Two shape parameters, related to axial and overall body thickness, predicted segment configuration with moderate to high success rate. We found that head morphology was a good predictor of its segment length. While there was a large variation in head segments, the length of tail segments was similar across all models. Given that fishes exhibited variable caudal fin shapes, the consistency of tail segments could be a result of an evolutionary constraint tuned for high propulsive efficiency. The bio-inspired multi-segment models presented in this study highlight the key bending points along the body and can be used to decide on the placement of actuators in fish-inspired robots, to model hydrodynamic forces in theoretical and computational studies, or for predicting muscle activation patterns during swimming.

1. Introduction

Undulatory swimming by fishes, where thrust is generated by the body and caudal fin through continuous, wave-like bending motions (Gray 1933, Bainbridge 1963), (Wardle *et al* 1995), (Di Santo *et al* 2021), has been a source of inspiration for underwater robotics for many years (Raj and Thakur 2016). Body bending kinematics in fishes varies with morphology (i.e. body geometry and stiffness), swimming speed and body size (Webb 1982), (Webb *et al* 1984), (Jayne and Lauder 1995), (Gillis 1997), (Tytell 2010), (Akanyeti and Liao 2013a). There have been numerous investigations exploring this kinematics diversity and studying underlying biomechanical and hydrodynamic mechanisms (Altringham and Ellerby 1999), (Lauder and Tytell 2005), (Shadwick and Lauder 2006) with the expectation of gaining novel insights into the ecological and evolutionary processes (Fish 1996), (Blake 2004), (Van Rees *et al* 2015), (Webb

1984), (Mu¨ller and van Leeuwen 2004), informing fisheries conservation and management (Tan *et al* 2021), (Castro-Santos *et al* 2009) and designing better robots (Zhong *et al* 2017), (Marchese *et al* 2014), (Katzschmann *et al* 2018), (Kruusmaa *et al* 2014).

Bio-inspired robots are often made from interconnected segments (Liu and Hu 2010), (Su *et al* 2014), (Low and Chong 2010), and it is a non-trivial problem to identify the optimal segment configuration (i.e. number of segments, relative length of each segment, and whether a given segment should be rigid or flexible) that allows the replication of undulatory swimming with high propulsive efficiency. Several methods have been proposed to estimate some of the design parameters automatically (Valdivia y Alvarado and Youcef-Toumi 2006), (Yu *et al* 2007), (El Daou *et al* 2014), (Karakasiliotis *et al* 2016), (Ozmen Koca *et al* 2018). These methods usually start with the analysis of body midline kinematics, either recorded from biological experiments or generated artificially using analytical models. They look for parsimonious segment configurations (minimum number of segments) that minimize the difference between actual and predicted midlines. These multi-segment models can then be transformed into actual robot designs with further theoretical considerations on mechanical properties of the body and how it interacts with the surrounding fluid.

To date, the segmentation methods have been applied to study one species at a time, and we have a limited understanding of how optimal segment configurations should vary with morphology across a diversity of fish species, swimming speeds and body sizes to maintain high swimming efficiency. This is a reasonable concern as robots may have different sizes, shapes, and ranges of swimming speeds than the biological counterparts that inspired their design. A systematic comparison of multi-segment models across multiple species could help begin to explore the design space more effectively and pave the way for more quantitative basis of bioinspired underwater robot designs.

With the general aim of bridging the gap between biology and robotics in the design of aquatic undulatory locomotor systems, here we present optimal segment configurations for a diverse group of fishes during steady swimming. We address the following questions: (1) how many segments are required to describe the bending kinematics accurately; (2) should these segments have equal or variable-length throughout the body; (3) how does segment configuration change with swimming speed and body size; (4) is there a connection between segment configuration and kinematics variables that are traditionally used to describe midline kinematics (e.g. tail beat amplitude, wavelength, and maximum body curvature); and (5) what is the relationship between segment configuration and body shape?

We also test whether optimal segment configurations can be partitioned into discrete categories as fishes that use undulatory swimming have been historically divided into four groups or swimming modes (i.e. anguilliform, sub-carangiform, carangiform and thunniform swimmers). The categorization of fishes into swimming modes is based on morphological traits and presumed patterns of midline kinematics (Breder 1926), (Lindsey 1978). However, our recent work (Di Santo *et al* 2021) has called the validity of this categorization into question by showing that undulatory movements in fishes represent more of a continuum rather than discrete modes.

The study presented in this manuscript continues probing into this topic using a new kinematics analysis approach. Our initial investigation using data from ten fish species (Fetherstonhaugh *et al* 2021) showed that each fish had a distinct segment configuration even though they are all classified as sub-carangiform swimmers. Here, we build on this initial investigation by extending the segment analysis to a new and much larger dataset including 44 species with representatives from all four swimming modes and covering a significantly wider range of body shapes, sizes, and speeds.

2. Methods

2.1. Dataset

Our dataset was collected at four sites: Harvard University (Lauder Lab), Whitney Laboratory for Marine Bioscience at the University of Florida (Liao Lab), University of Rhode Island's Greenfins Tuna Facility and U. S. Geological Survey's S.O. Conte Anadromous Fish Research Centre (Conte Lab), and has been previously published (Goerig *et al* 2021).

The dataset includes 151 steady swimming video sequences from 44 species (43 fish species and one species of fish-like chordate, *Branchiostoma lanceolatum*). It consists of swimmers from all four classic swimming modes: anguilliform (23%), sub-carangiform (55%) carangiform (16%) and thunniform (6%), and covers a wide range of Reynolds numbers ($Re = 440–5.7 \times 10^6$) including both laminar and turbulent regimes where body length (L) and swimming speed (U) varied between $L = 0.3$ m–1.1 m and $U = 0.01$ m s^{-1}–7.4 m s^{-1}, respectively (figure 1(a)).

All swimming sequences were filmed using a high-speed camera with a sampling rate of 120 frames per second or higher. For each sequence, at least ten frames from one tail beat were digitized to obtain full body midline kinematics. All body midlines consisted of 200 equally spaced x and y coordinates where the first (x_1, y_1) and last (x_{200}, y_{200}) coordinates corresponding to the most anterior (snout) and posterior (tail tip) midline points, respectively. All midline points were normalized to L.

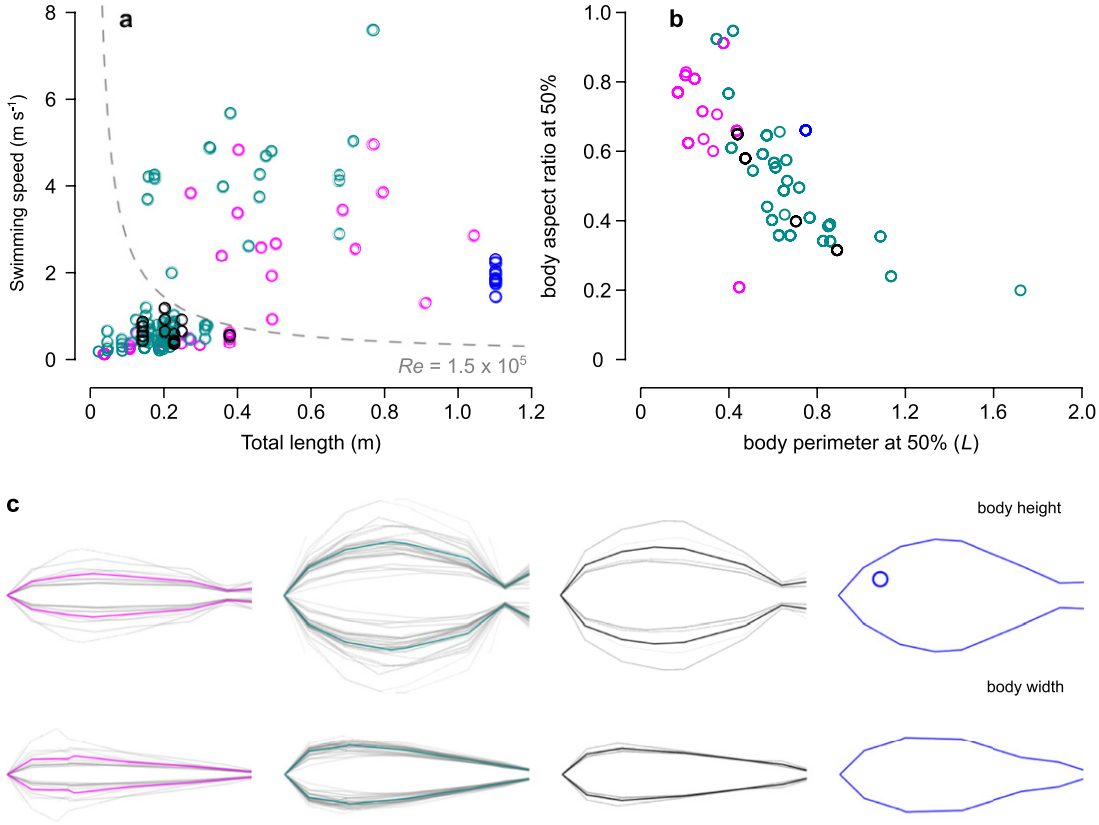

Figure 1. Dataset used in this study. (a) Distribution of individual data points (circles) across swimming speed (y-axis) and body length (x-axis). Color codes swimming mode; anguilliform (magenta), sub-carangiform (teal), carangiform (black) and thunniform (blue). During analysis, data points were divided into two groups, low Re ($< 1.5 \times 10^5$) and high Re ($> 1.5 \times 10^5$) (grey dashed line). (b) Distribution of individual data points in morphological space (one data point per species): x-axis and y-axis show perimeter (estimated as an ellipsoid) and AR (width divided by depth) of the body at 50% SL. (c) Silhouettes of all fish species from lateral (top panels) and dorsal views (bottom panels) showing body height and width, respectively. All measurements are shown in grey. Mean silhouette for each swimming mode (color-coded) is also shown.

The dataset also includes measurements of body shapes for all tested species which were obtained independently from museum specimens (Di Santo *et al* 2021). Measurements were taken from side (lateral) and top (dorsal) views to estimate body width (b_w, thickness along left-right axis) and depth (b_d, height along ventral-dorsal axis) at various locations along the body: 10%, 25%, 50% 75% 90% and 100% standard length (SL). From these, we calculated aspect ratio (AR) and perimeter length around the anterior–posterior axis (P) using equations (1) and (2), respectively,

$$\mathrm{AR} = \frac{b_w}{b_d} \tag{1}$$

$$P = 2 \times \pi \times \sqrt{\frac{b_w^2 + b_d^2}{8}} \tag{2}$$

AR varied between 0.45–4.80 at 10%, 0.27–1.12 at 25%, 0.19–0.95 at 50%, 0.12–0.93 at 75%, 0.25–1.58 at 90% and 0.15–0.86 at 100% SL. P varied between 0.13–0.84 at 10%, 0.17–1.40 at 25%, 0.16–1.73 at 50%, 0.14–1.47 at 75%, 0.09–0.36 at 90% and 0.04–0.38 at 100% SL (distribution of data points at 50% SL is shown in figure 1(b)). These measurements as well as body silhouettes (figure 1(c)) highlight the morphological diversity of fishes included in the dataset.

2.2. Estimation of multi-segment models

We employed the segment growing method (SGM) proposed in (Fetherstonhaugh *et al* 2021) to generate a multi-segment model ($\hat{M}$) which describes the fish body midlines (M) as a series of linear (rigid) segments (s) connected with joints (j).

Briefly, starting from the most anterior midline point (x_1, y_1), the first segment (s_1) was created with an initial length $0.005L$ and grown with $0.005L$ increments until the segment error, E_1, exceeded a threshold value defined by the user *a priori* ($0.01L$). When E_1 exceeded the threshold, $s_1$was stopped growing and fixed with a joint (j_1) at the end. Next, the second segment (s_2) was created with the same initial length and this time was grown from j_1 until the error (E_2) between the segment and the midline exceeded the threshold. This iterative process continued until the most posterior midline point along the body was reached. At the end, the SGM produced a parsimonious multi-segment model (SGM model

herein after) which consisted of segments with variable lengths, each of which described a finite portion of the actual midline.

The accuracy (A) of a SGM model was then defined as percentage of L based on the maximum segment error in the model:

$$A = 100 \times \left(1 - \max_{i \in \hat{M}} E_i\right) \tag{3}$$

where i is the index of all segments found in the SGM model $\hat{M}$. The error for segment i, E_i, was calculated using

$$E_i = \frac{1}{t}\sum_{t=1}^{T} D_i(t) \tag{4}$$

where $D_i(t)$ is the maximum perpendicular distance between the segment line and actual midline curve. $D_i(t)$ was estimated independently for each time frame, t, and then averaged over the entire tail beat cycle, T.

The user-defined threshold controls the tradeoff between the accuracy and the complexity of a SGM model. The smaller the threshold, the more accurate the model is however, it also becomes more complex by having more segments. The $0.01L$ threshold value, used in this study, was determined using a trial-and-error process after preliminary testing on multiple datasets (figure 2(a)). The more detailed description of how SGM works was presented in (Fetherstonhaugh *et al* 2021).

2.3. Data analysis

Custom-written Matlab scripts were used to implement the SGM and analyze all data.

2.3.1. Comparison with equal-length segment models

The performance of SGM models was compared to models consisting of equal-length segments, where segment joints are distributed evenly across the body. Equal-length segments are common in robots described in the literature (Yu *et al* 2007); especially while designing the posterior body (Liu and Hu 2006), (Ay *et al* 2018). Relative difference in performance (ΔA) was calculated using,

$$\Delta A = 100 \times \left(\frac{A_v - A_e}{A_v - A_s}\right) \tag{5}$$

where A_v A_e and A_s correspond to the accuracies of SGM, equal-length segment and single-segment models. A single segment model represents the worst-case scenario where body midlines were represented with a single segment like a rigid plate (i.e. for each frame a line was drawn to connect the first and last midline points). Here, the difference between A_v and A_s was used as a baseline against which the difference between A_v and A_e was compared.

We predict negative correlation between ΔA and number of segments, i.e. ΔA will be large in models with fewer segments and it will decrease as number of segments increases (i.e. $\Delta A \to 0$). Multiple T-tests with Bonferroni correction were performed to evaluate whether ΔA was statistically different from 0.

2.3.2. Analysis of segment configuration

In all models, segment configuration was evaluated using several parameters: number of segments, relative length of head segments (s_{head}), relative length of tail segments (s_{tail}), and segment length variability along the body. The segment length variability was measured using coefficient of variation (CV),

$$\text{CV} = \frac{\delta}{\mu} \tag{6}$$

where μ and δ are the mean and standard deviation of segment lengths in the model. The higher the CV, the higher the variability (CV $=$ 0when the model had equal-length segments). Length ratio ($R_{\text{h:t}}$) between head and tail segments was also measured ($R_{\text{h:t}} = 1$ when lengths of head and tail segments were equal),

$$R_{\text{h:t}} = \frac{s_{\text{head}}}{s_{\text{tail}}} \tag{7}$$

CV and $R_{\text{h:t}}$ were plotted to study how segment length variability changed with increasing number of segments, and multiple T-tests with Bonferroni correction (one test per segment number) were performed to evaluate whether mean values were significantly different from equal-length segment scenario (i.e. CV $=$ 0and $R_{\text{h:t}} = 1$). We predict that there will be more variability in models with fewer segments (i.e. CV $\gg$ 0and $R_{\text{h:t}} \gg 1$), and it will decrease as number of segments increases (i.e. CV $\to$ 0 and $R_{\text{h:t}} \to 1$).

2.3.3. Relationship between segment configuration and swimming kinematics

Assuming that there is an association between the bending kinematics of fishes and the segment configuration of their respective SGM models, we measured the correlation (r) between kinematic variables (i.e. tail beat frequency, body wavelength, head oscillation amplitude, tail oscillation amplitude, ratio of head:tail oscillation amplitude, maximum curvature and maximum curvature location along the body) and segment configuration variables (i.e. segment number, s_{head}, s_{tail}, CV and $R_{\text{h:t}}$). The methods used to calculate the listed kinematic variables are described in (Di Santo *et al* 2021). We predict that fishes undulating along the entire body will require more segments than those whose bending movements are restricted to the posterior body. We also predict that fishes with greater head oscillations will have shorter head segments. Similarly, we can assume that fishes with greater tail oscillations and maximum body curvature will have a higher segment length variability along the body, i.e. posterior segments will be shorter than the anterior segments to accommodate for higher body curvatures towards the tail.

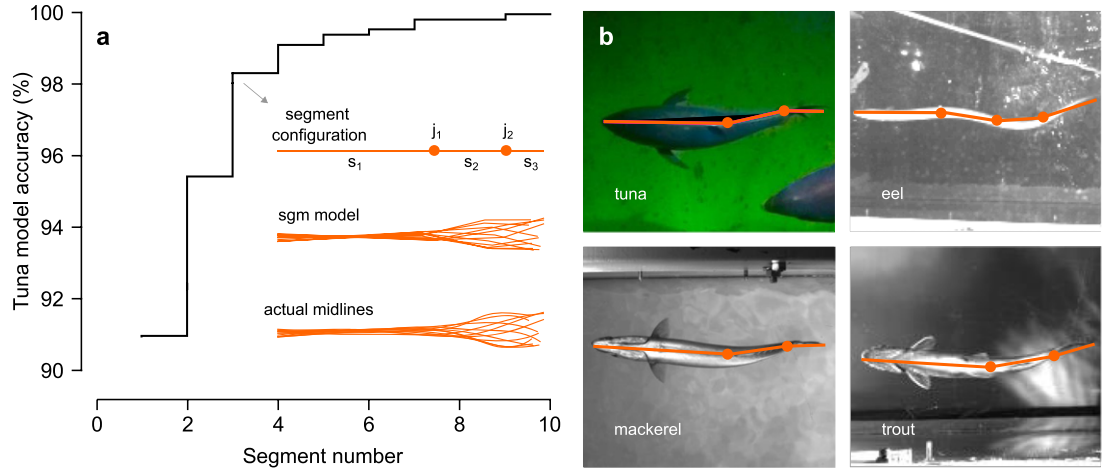

Figure 2. (a) Overall SGM model accuracy versus segment number for one representative fish; yellowfin tuna (*T. albacares*, $L = 110$ cm, $U = 1.6L$ s^{-1}). Midlines generated by the three-segment model mimics the actual tuna midlines with more than 98% accuracy. Segment configuration of the model is also shown where s_1 and s_3 correspond to head and tail segments, respectively, and j_1 and j_2 show joint positions connecting three segments (i.e. s_1 and s_2, and s_2 and s_3). (b) SGM models superimposed on actual video frames: (top left) tuna from the same video sequence presented in (a); (top right), American eel (*A. rostrata*, = 38 cm, $U = 0.7L$ s^{-1}); (bottom left) mackerel (*S. scombrus*, = 23 cm, $U = 1.3L$ s^{-1}); (bottom right) brook trout (*S. fontinalis*, = 19 cm, $U = 0.8L$ s^{-1}).

We also looked at whether *a priori* grouping of fishes into distinct swimming categories or modes as described in (Breder 1926), (Lindsey 1978) would help explaining the variations seen in the of segment configurations of SGM models. These categories were originally proposed based on kinematic differences observed in key species (e.g. eel for anguilliform and tuna for thunniform swimmers), and were assumed to describe the kinematic diversity of all fishes (hereinafter distinct swimming modes hypothesis). If this hypothesis is correct, the segment configuration of the SGM models will vary based on swimming mode; anguilliform, sub-carangiform, or thunniform. Eel-like fishes (i.e. anguilliform swimmers) having more flexible and elongated bodies will require more segments than fishes with relatively stiff body anatomy (i.e. carangiform swimmers). Conversely, fishes with longest wavelength due to a more rigid anatomy will require the fewest segments (i.e. thunniform swimmers). However, our recent kinematics analysis on multiple species has challenged this view (Di Santo *et al* 2021). We found quite a few examples of fishes sharing similar kinematic patterns although assigned to different swimming modes, and vice versa (fishes adopting different kinematic patterns although assigned to a same swimming mode). In this case, we may not see recognizable differences between SGM models assigned to different modes.

We used Kruskal Wallis tests to compare segment number in SGM models and one-way analysis of variance to compare other segment configuration parameters, followed by Tukey–Kramer multiple comparison tests. We performed the statistical analysis twice using two different data sets. First, we compared SGM models of four canonical species traditionally used to define the classic fish swimming modes: American eel—*Anguilla rostrata*—anguilliform, brook trout—*Salvelinus fontinalis*—sub-carangiform, mackerel—*Scomber scombrus*—carangiform, and tuna—*Thunnus albacares*—thunniform (figure 2(b)). This analysis included 40 video sequences (ten per species). Second, we repeated our analysis on the entire data set, where we assigned each species to one of four swimming modes based on common use in the existing literature.

2.3.4. Relationship between segment configuration and Reynolds number

It has been previously shown that scaling laws governing the undulatory movements of aquatic swimmers may vary between laminar and turbulent regimes (Gazzola *et al* 2014), (Tytell *et al* 2016), (Smits 2019) which are characterized by Reynolds number, Re,

$$\mathrm{Re} = \frac{\rho U L}{\mu} \tag{8}$$

where ρ is the density of the fluid, and μ is the dynamic viscosity.

We hypothesize that the SGM models will have more segments and less length variability at high Re when body amplitudes increase anteriorly (Akanyeti *et al* 2017). To test this hypothesis, SGM models were divided into two groups using a threshold, $\mathrm{Re}_{\mathrm{threshold}} = 1.5 \times 10^5$: group 1 consisted of models representing data points with low Re ($\mathrm{Re} < \mathrm{Re}_{\mathrm{threshold}}$) and group 2 consisted of models representing data points with high Re ($\mathrm{Re} > \mathrm{Re}_{\mathrm{threshold}}$). Here, $\mathrm{Re}_{\mathrm{threshold}}$ was determined after analyzing the distribution of data points in figure 1(a). Kruskal Wallis and Tukey–Kramer multiple comparison tests were used to compare segment

numbers between the two groups. One-sample Kolmogorov Smirnov test was performed to evaluate whether segment configuration parameters (s_{head}, s_{tail}, $R_{h:t}$ and CV) came from normal distributions in each group. The null hypotheses were rejected at 5% significance level, i.e. the distributions were not normal. Hence, the non-parametric Wilcoxon rank sum test was performed to evaluate whether their mean values were different at 5% or less significance level.

2.3.5. Relationship between segment configuration and morphology

We first checked whether body shape could predict the size of SGM models. Linear discriminant analysis classifier (LDA-classifier) was trained to predict segment number using an input vector consisting of shape measurements AR and P (multiple measurements along the body as described in section 2.1). The performance of the LDA-classifier was evaluated based on the percentage of correctly classified instances. For instance, if a model had three segments and the LDA-classifier predicted the same number, this would correspond to a correctly classified instance. The confusion matrix, a table summarizing the prediction results, was also visualized to investigate incorrectly classified instances. We then looked at whether body shape could predict segment lengths and variability. Multiple linear regression model (MLR-model) was fitted to predict segment configuration parameters (s_{head}, s_{tail}, $R_{h:t}$ and CV) using the same input vector described above. The performance of the MRL-model was evaluated using the coefficient of determination (r^2). To evaluate the interactions between Re, body shape and segment configuration, LDA and MLR analysis were repeated three times: (1) using low Re models in the first group, (2) using high Re models in the second group, and (3) using all SGM models.

3. Results

All results are reported as mean ± standard deviation for continuous variables (e.g. s_{head}), and median (interquartile range) for discrete variables (e.g. segment number).

3.1. Accuracy and segment configuration of SGM models

The mean accuracy of the SGM models was above 95% (figure 3(a)), and 83% of the SGM models had fewer than five segments (figure 3(b)). In general, the SGM models performed significantly better than equal-length segment models with an improvement close to 50% in two-segment, 30% improvement in three-segment and 15% improvement in four-segment models; after that there was no significant difference between SGM and equal-length segment models (supplementary figure 1 (https://stacks.iop.org/BB/17/046007/mmedia)).

The mean joint positions and segment configuration of the SGM models are presented in supplementary tables 1 and 2, respectively. While s_{head} became shorter with increasing number of segments, s_{tail} mostly stayed the same; confined posteriorly in the last 20% of the body (figures 4(a) and (b)). Head segments were consistently longer than the tail segments regardless of the number of segments in the model. All $R_{h:t}$ values were significantly higher than the baseline where $s_{head} = s_{tail}$ (figure 4(c)). Similarly, anterior segments were longer than the posterior segments. Again, all CV (representing the variability in segment length) values were significantly higher than the baseline where all segments had equal length (figure 4(d)).

3.2. Relationship between segment configuration and swimming kinematics

There was a correlation between kinematic variables and the segment configuration of the SGM models (table 1). Most notably, the models representing fishes with higher oscillation amplitude and frequency had more segments, shorter s_{head} as well as lower $R_{h:t}$ and CV. Posterior–anterior shift of the maximum curvature point along the body (towards the head) had a similar effect on the segment configuration (i.e. more segments and less variability). In addition, fishes with longer propulsive wave required fewer segments but the correlation between wavelength and segment number was not as high.

We next compared the SGM models of four species each of which was a representative of a swimming mode. We found that the segment configuration of the eel models was different than the rest: eel models had more segments and shorter s_{head} than the trout, mackerel, and tuna models, as well as lower $R_{h:t}$ and CV than the trout models (supplementary table 3). We found similar results, when the analysis was extended to all species. The anguilliform models and to a lesser extent the sub-carangiform models were likely to have more segments than the models representing the other two swimming modes (supplementary figure 2). The anguilliform models also had shorter s_{head} and lower $R_{h:t}$ and CV (figure 5). In both datasets, s_{tail} length did not change between the swimming modes (supplementary table 3 and figure 5(b)).

3.3. Relationship between segment configuration, Re and morphology

The separation of the anguilliform models from others was not related to speed or body length as the mean Re was only significantly higher in the thunniform models. We next split the SGM models into two groups (low versus high Re) and compared their segment configurations. The high Re models had shorter s_{head} as well as lower $R_{h:t}$ and CV compared to the low

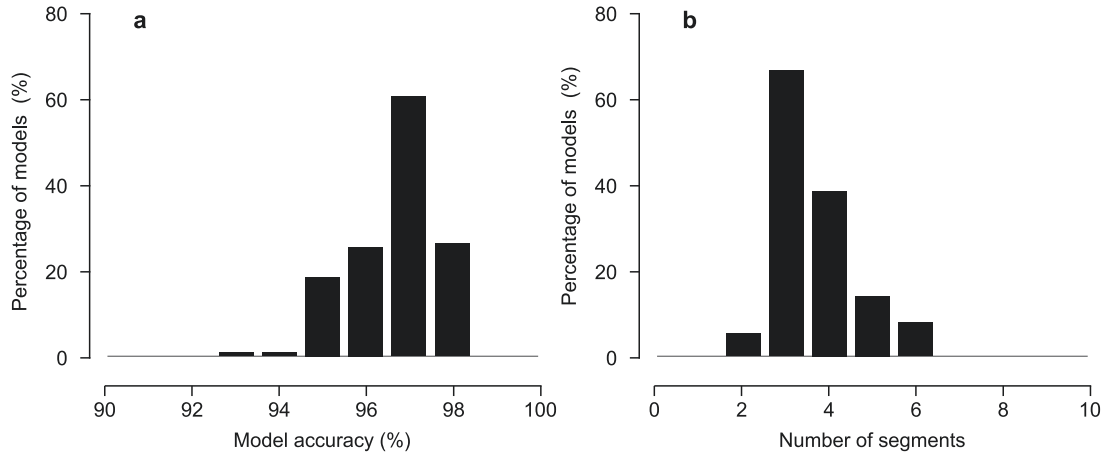

Figure 3. (a) Histogram of the SGM models' accuracy. The mean accuracy was 97.2 ± 0.9% with minimum and maximum values of 93.4% and 98.4%, respectively. (b) Histogram of the SGM models' segment number (3[3–4]): 4% (two-segment models), 50% (three-segment models), 29% (four-segment models), 11% (five-segment models) and 6% (six-segment models).

Table 1. Correlation coefficients between kinematics and segment configuration variables. Markers † and * indicate statistical significance at $p < 0.001$ and $p < 0.05$, respectively.

	Seg. No.	s_{head} (L)	s_{tail} (L)	$R_{h:t}$	CV
Tail beat freq.	0.30†	−0.44†	0.03	−0.35†	−0.45†
Body wavelength	−0.24†	0.13	0.07	0.04	0.07
Head amplitude	0.50†	−0.50†	−0.07	−0.33†	−0.40†
Tail amplitude	0.53†	−0.49†	−0.10	0.32†	−0.40†
head:tail ratio	0.37†	−0.48†	−0.03	−0.32†	−0.40†
Max. curvature	0.17*	−0.10	−0.22†	0.14	0.06
Max. curv. location	−0.31†	0.28†	−0.07	0.22†	0.17*

Re models. The high Re models also had one more segment than the low Re models, though this difference was not statistically significant (supplementary table 4).

The segment configurations of both low and high Re models were closely associated with body shape. 86% of the segment number predictions were correct for the LDA-classifier trained and tested on low Re models, and 78% for the LDA-classifier trained and tested on high Re models. Both classifiers had maximum prediction error of one segment in all incorrectly classified instances (see confusion matrix tables in figure 6(a)). For both classifiers, the class means of the input shape parameters (AR and P) are presented in supplementary table 5. The performance of the multi linear regression models linking body shape to other segment configuration variables were moderate to high (actual versus predicted s_{head} is shown in figure 6(b) as an example), except for s_{tail} where no significant association was found. The analysis of coefficients (presented in supplementary table 6) indicated that the shape parameters within the first and last quarter of the body (around head and tail regions) significantly contributed to the overall performance of the MLR-models. When LDR-classifiers and MLR-models were trained and tested on the entire dataset (without Re separation), the associations were still significant, but the predictive performance dropped by 16% (segment number), 55% (s_{head}), 45% ($R_{h:t}$), and 48% (CV). This suggests that the relationship between segment configuration and body shape may depend on Re and thus vary between laminar and turbulent flow regimes.

4. Discussion

We analyzed the steady swimming kinematics of a large group of freshwater and marine fish species with vastly different morphologies. To the best of our knowledge, this is the most comprehensive dataset available on fish kinematics and covers a wide range of speeds, body lengths and all four classically defined swimming modes. We used a novel approach to model the midline kinematics of every individual as a series of interconnected segments, i.e. SGM which is described in detail in (Fetherstonhaugh *et al* 2021). Compared to more traditional midline analysis methods, such as measuring Strouhal number (Taylor *et al* 2003), optimal specific wavelength (Nangia *et al* 2017), or describing body amplitude envelope using nonlinear regression fits (Di Santo *et al* 2021), the SGM models provide pragmatic design guidelines

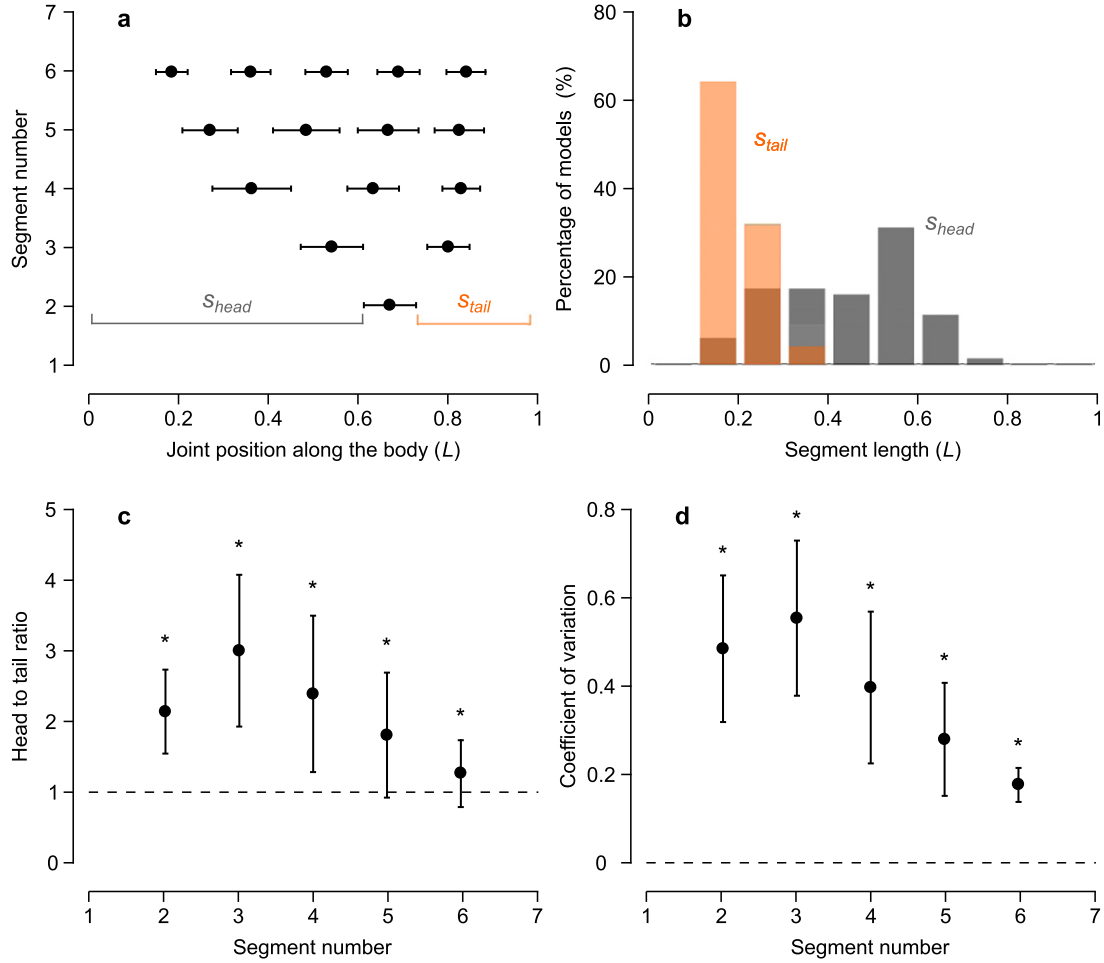

Figure 4. (a) Mean joint positions for two, three, four, five and six-segment SGM models. Horizontal error bars indicate one standard deviation from the mean. (b) Histogram of head (grey) and tail (orange) segment lengths. (c) Length ratio between head and tail segments ($R_{h:t}$) across models with different segment numbers. $R_{h:t} = 1$ is plotted as a reference for equal-length segment model (dashed line). (d) (CV measuring segment length variability along the body) across models with different segment numbers. CV = 0 is plotted as a reference for equal-length segment model (dashed line). In both (c) and (d), marker * indicates data points which are higher than the baseline at a significance level, $p < 0.01$, and vertical error bars indicate one standard deviation from the mean.

for articulated robots. By highlighting the key bending points along the body, the SGM models can be used in a variety of applications. For example, they can orient the placement of actuators in fish-inspired robots, compare midline kinematics between robots and fishes, estimate hydrodynamic forces in theoretical and computational studies, and predict muscle activation patterns in fishes.

During analysis of SGM models, we mainly focused on comparing the lengths of first (head) and last (tail) segments as both segments are considered to play a key role in propulsion (Anderson *et al* 1998), (Van Buren *et al* 2019), (Lucas *et al* 2020), (Lighthill 1993), (Akanyeti *et al* 2017). Plus, all models had a head and tail segment irrespective of whether they had two or six segments. We also studied the segment length variability of models, whether they had equal-length or variable-length segments. We evaluated variability using two metrics, the length ratio between head and tail segments and the CV, which allowed us to compare models with different segment numbers objectively. Because there is a finite body length, more segments would constrain the variation of each more so than fewer segments. By evaluating variability in relation to mean segment length, the CV provided a more robust statistical measure than alternatives such as standard deviation.

Our results show that steady swimming kinematics in fishes can be successfully described with a limited number of rigid segments (up to six). The majority of the SGM models (83%) were made from four or fewer segments, and in these models, the anterior segments were longer than the posterior segments. These are encouraging findings for engineers as technological constraints often limit the number of segments used in multi-segment robots due to the complexity and cost of adding actuators to connect adjacent segments. Previous studies have already shown that the segment numbers can be further reduced by designing hybrid robots which are made of rigid anterior and flexible posterior segments (Low and Chong 2010), (White *et al* 2021). In this design

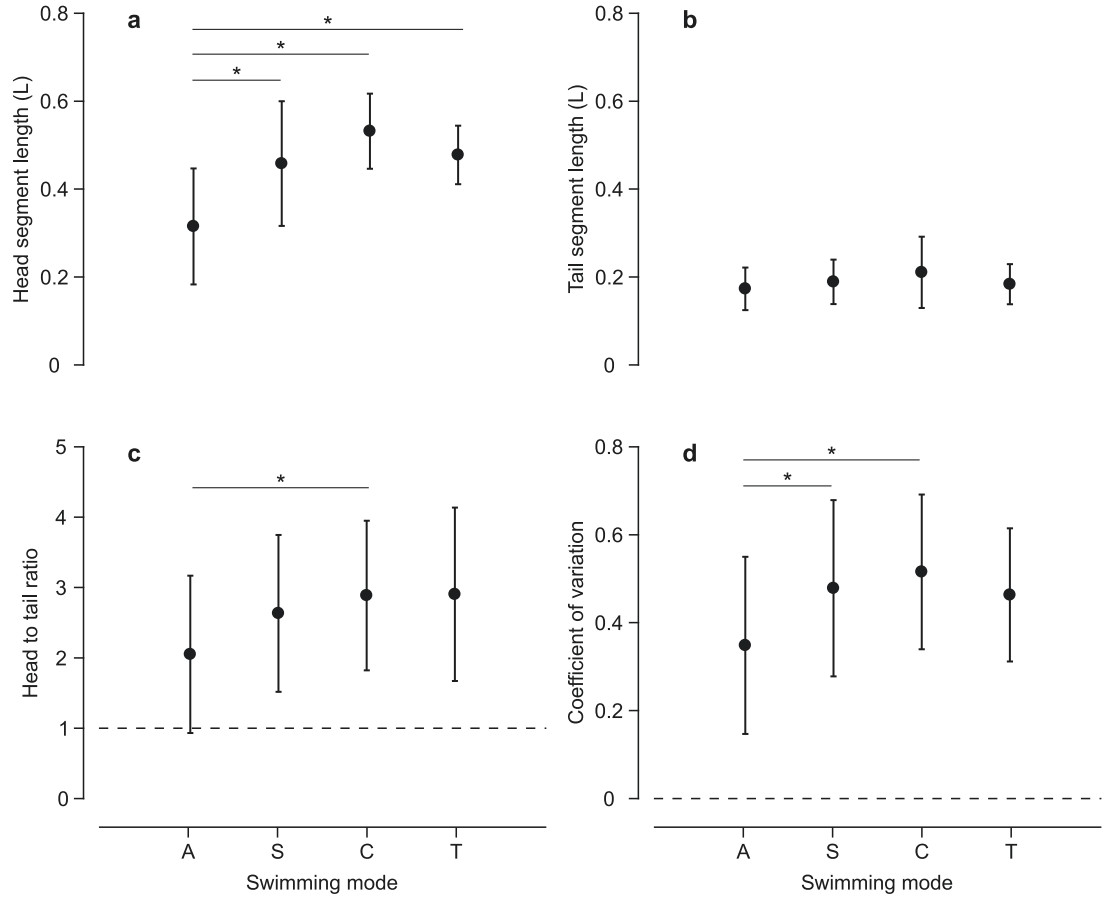

Figure 5. Models' segment configuration versus swimming mode. A, anguilliform; S, sub-carangiform; C, carangiform; T, thunniform. (a) Head segment length (s_{head}). (b) Tail segment length (s_{tail}). (c) Length ratio between head and tail segments ($R_{h:t}$). (d) CV. Error bars indicate one standard deviation from the mean (circle). Marker * indicates statistical significance at $p < 0.01$. Horizontal dashed lines in (c) and (d) show baseline $R_{h:t} = 1$ and CV $= 0$ values (equal-length segment model).

approach, the anterior segments are often used to house batteries, electronics, sensors, and actuators of the robot, although in recent years there has been significant push to design robots with more evenly distributed sensing and actuation capabilities (Venturelli *et al* 2012), (Thandiackal *et al* 2021), (Jusufi *et al* 2017), (Rossi *et al* 2011).

Overall, the SGM models had highly variable segment configurations, and we investigated whether these variations could be linked to swimming kinematics, morphology and Re. The key findings are discussed below.

4.1. Weak association between segment configuration and body wavelength

Kinematic variables, head and tail amplitude, maximum curvature and body wavelength all contributed to the segment configuration of the SGM models, though not as much as expected (table 1). Most notably, our initial hypothesis that fishes with longer wavelength will require fewer number of segments was not confirmed, the correlation between the two variables was weak. For instance, all SGM models derived from brook trout had three segments (except one with four segments) even though the wavelength between individual data points varied to a great extent (from $0.63L$ to $1.37L$ with mean$0.95 \pm 0.22L$). We also did not find any correlation between body wavelength and head segment length. We believe that the length of head segment is a good indicator of where the undulatory wave is initiated because its joint with the vertebral column approximates the first bending point along the body.

4.2. Distinct segment configuration in anguilliform models

The common view that fish locomotion can be categorized into distinct swimming modes has been very influential in fish-inspired robotics research (Sfakiotakis *et al* 1999). We have recently shown that there are no clear boundaries between swimming modes, and often fishes exhibit similar midline kinematics regardless of assigned swimming mode (Di Santo *et al* 2021). In that study, we proposed that the categorization of swimming modes relates to morphological traits rather than actual bending kinematics. Apart from anguilliform swimmers having significantly shorter wavelength than species classified in other modes, we did not find any significant differences between groups when key kinematic

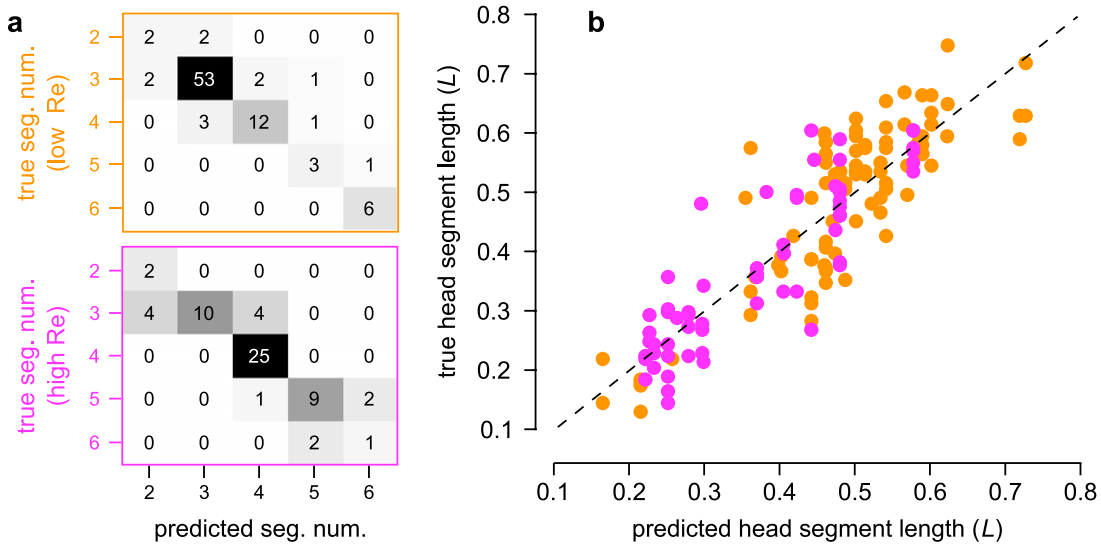

Figure 6. Relationship between morphology and segment configuration at low Re ($<= 1.5 \times 10^5$, purple) and high Re ($>1.5 \times 10^5$, orange). (a) Segment number prediction using linear discriminant analysis. Confusion matrix tables showing true (row) and predicted (column) segment numbers. Numbers in the diagonal cells show correctly classified data points. Grey color map indicates distribution of data points across the table (darker colors corresponding to higher percentages). Overall, percentage of correctly classified data points are 86% (low Re) and 78% (high Re). (b) Head segment length prediction using multiple linear regression analysis. r^2 values are 0.70 (low Re) and 0.76 (high Re) at a significance level, $p < 0.01$. Circles show individual data points. Ideal prediction, ($y = x$, dashed line) is also plotted as a reference.

parameters (ratio between head and tail oscillations, body curvature, and amplitude and phase envelopes) were compared.

Our results here also do not support the distinct swimming mode hypothesis, particularly with regard to the sub-carangiform, carangiform and thunniform swimming categories. The SGM models did not significantly vary across swimming modes except for models describing anguilliform swimmers. The anguilliform models had more segments and less segment length variability along the body, suggesting that anguilliform swimmers recruit the anterior portion of their body to a greater extent than other species. Anguilliform models also had shorter head segments, suggesting that the undulatory body wave is initiated more anteriorly in anguilliform swimmers. Our results also show that the length of the tail segment did not change as much across the models, and the tail joint was around the last fifth of the body (except in models with two segments). Although different fish species exhibit a variable caudal peduncle (the region where caudal fin attaches to the body) in thickness and tail fin shape (Lauder 2000), the consistency of tail segments in SGM models suggests that fishes may move their caudal fins in a similar way (at least in two dimensions), which may be a result of common adaptation to improve propulsive efficiency. With multiple short segments in the posterior body region (i.e. higher degrees of freedom), it should become easier to control the angle and amplitude of the tail so that the momentum of the undulatory wave can be transferred into the fluid more effectively.

4.3. Strong association between segment configuration and body shape

We found a strong association between shape and the configuration of SGM models. Over 70% of the variability in segment number and length of head segments, and more than 35% of the variability in segment length of the models is explained by two shape parameters measured at different locations along the body: AR and perimeter length. We chose to consider these two parameters because they are correlated with bending stiffness. AR is indicative of relative body thickness along the medial-lateral (bending) axis, while perimeter length estimates overall body thickness. All else being equal, bending stiffness should increase with increasing AR and perimeter. We speculate that the association between shape and SMG models would be even stronger if we had shape measurements for every individual in the dataset.

Fishes also exhibit a large diversity of head morphologies, which affects flow sensing (Chambers *et al* 2014), (Yanagitsuru *et al* 2018) and feeding performance (Carroll *et al* 2004). In contrast, we know less about how head morphology affects bending kinematics and swimming performance (Rouleau *et al* 2010), (Langerhans 2009). In this study, we found that, at low Re, the head shape was closely related to the segment configuration of the SGM models (supplementary table 6). The models describing fishes with relatively thicker heads (e.g. Atlantic spadefish—*Chaetodipterus faber*, perimeter at 25% of body length, $P_{25} = 1.01L$) had longer anterior segments

($s_{head} = 0.63L$) and higher segment length variability ($R_{h:t} = 0.79$and CV $= 4.67$) than models describing fishes with thin heads (e.g. American eel, *A. rostrata*, $s_{head} = 0.16L$, $R_{h:t} = 0.18$and CV $= 0.64$). In fish biomechanics literature, we often find simpler measurements of body shape (e.g. maximum depth, width, and their positions along the body) being reported. When we retrained the MLR-model for s_{head} prediction using only these simpler measurements, its performance dropped by more than 50%, highlighting the utility of more comprehensive morphometric measurements (including head shape).

Our dataset consisted of elongated (e.g. Atlantic hagfish—*Myxine glutinosa*), fusiform (e.g. brown trout—*Salmo trutta*) and deep-bodied fishes (e.g. sheepshead—*Archosargus probatocephales*) (i.e. no dorsoventrally compressed fishes). The SGM models describing elongated fishes (high AR and low perimeter) had higher segment numbers, their head segments were shorter, and they had equal segments along the body in comparison with the SGM models describing fusiform (moderate AR and moderate perimeter length) and deep-bodied fishes (low AR and high perimeter). However, there were a few outliers. For instance, the models describing elongated inshore lizardfish (*Synodus foetens*), had relatively low segment numbers (three to four) and long head segments (covering more than 40% of the body). Similar observations were made previously for models describing other elongated fishes such as Northern barracuda (*Sphyraena borealis*) and Florida gar (*Lepisosteus platyrhincus*) (Fetherstonhaugh *et al* 2021). These fishes are considered to have high flexural stiffness (Long and Nipper 1996) (Long *et al* 1996), and it was likely that the SGM models describing stiff fishes had overall fewer segments than those describing flexible fishes. Although shape is a key determinant, other factors including internal anatomy (e.g. number of vertebrae) and muscle activation patterns of fishes influence the resultant undulatory kinematics; hence, we expect that the segment configuration of SGM models would also depend on these factors. In addition, knowing more about these factors will help engineers design better robots; for example, while deciding on the material properties of segments (e.g. length, weight, and modulus of elasticity) and how they are actuated.

4.4. Segment configuration in laminar and turbulent regimes

Our dataset consists of fishes swimming in the inertial regime (Re $\gg 1$). The boundary layer of inertial swimmers is governed by either laminar or turbulent flows where transition from laminar to turbulent is expected to occur at Re between 10^3–10^5 (Anderson *et al* 2001). Previous studies have shown that scaling relations, linking kinematics to speed and size, are different between the two regimes due to the type of drag dominating each regime; skin friction drag in laminar flows and pressure drag in turbulent flows (Gazzola *et al* 2014). In our study, we found a similar dichotomy between the SGM models at low and high Re. The low Re models had fewer segments with longer head segments, and higher segment length variability along the body than high Re models. Recruitment of anterior body at high Re could be an adaptation to reduce pressure drag or boost thrust (Lighthill 1969), (Gemmell *et al* 2016), (Akanyeti *et al* 2017), (Lucas *et al* 2020). Alternatively, it could be related to improving other functions such as sensing and respiration (Akanyeti *et al* 2016). Likewise, while predicting segment configuration in relation to body shape, we achieved higher performance by training a separate classifier/regression model for each Re group.

In our analysis, we used $Re_{threshold} = 1.5 \times 10^5$ to split the data between low and high Re, which was an order of magnitude higher than the threshold used in (Gazzola *et al* 2014); i.e. 10^4. Repeating our analysis using that lower threshold did not improve the prediction performance; on the contrary, we saw a significant drop at high Re (e.g. from $r^2 = 0.70$ to $r^2 = 0.36$ in head length prediction), and the results at low Re were inconclusive as there were only nine data points with Re $< 10^4$. The differences in the four experimental setups (which were used to collect the dataset analyzed in this study) may be a plausible explanation for the higher $Re_{threshold}$ having a better fit in the current analysis. With this threshold, the high Re group mostly consisted of data points collected at the Conte Lab. Compared to the other three setups which were geared toward measuring sustained swimming ability in laboratory settings, the Conte Lab's experimental flume allowed fishes to swim at volitional high speeds in more natural conditions (Castro-Santos 2005).

5. The future of multi-segment models

Our work shows that multi-segment models with six or fewer rigid segments are sufficient to describe the undulatory kinematics of fishes, that the anterior segments of the models are typically longer than their posterior segments, and that the segment configuration of the models are highly variable depending on the Re, swimming pattern, and body morphology of fishes. We also show that this variability cannot be explained by a priory grouping of fishes into distinct swimming modes. These findings have two main implications for future fish-inspired robot designs. First, the geometry and Re of a robot should be considered *a priori* before deciding how to partition its body into segments, especially in the anterior part. A fusiform robot swimming at low Re may need to be more streamlined with a long head segment to reduce drag, whereas an elongated robot swimming at high Re may require shorter head segments

to produce thrust. In contrast, we see more alignment in the posterior portion of the SGM models, where segments progressively get shorter to account for increased body curvatures toward the tail. Several studies have already shown that this specific posterior segment configuration may improve the swimming performance of freely swimming robots (Yu *et al* 2007), (White *et al* 2021).

Second, the segment configuration of many fish robots is determined based on artificial midlines generated by the sinusoidal travelling wave equation. This equation is assumed to approximate actual fish midlines reasonably well at least during steady swimming (Tytell and Lauder 2004) and Kármán gaiting (Akanyeti and Liao 2013b), and it is commonly used in numerical simulations to study fish locomotion (Borazjani and Sotiropoulos 2008, Borazjani and Sotiropoulos 2009), (Li *et al* 2021). The equation takes two input parameters (amplitude envelope and wavelength) to generate proto-midlines tailored for different swimming modes; for instance, wavelength $= 0.5L$ for anguilliform swimmers and $1L$ for carangiform swimmers. Our results show that this simplified approach is not sufficient to capture all the kinematics diversity observed in steady swimming of fishes, and propulsive wavelength is not a good predictor of the key bending points along the body. We argue that the performance of fish-inspired robots will improve if they are designed based on real fish kinematics and morphometric measurements, and this approach has been applied recently for the construction of a tuna-inspired robot (White *et al* 2021). We provide SGM models (supplementary table 7) to be used in fish-inspired robotic platforms. In addition, data-driven classifier and regression models presented in this study (supplementary tables 5 and 6) will enable robotics researchers to determine optimal segment configurations for body shapes and Re that are not listed in supplementary table 7.

5.1. Limitations and future work

There are several limitations to our study. First, our analysis considers only steady swimming kinematics, and it is unclear how SGM models may differ when modelling unsteady swimming kinematics (e.g. turn, acceleration, escape and station holding in turbulent flows, see (Domenici and Blake 1997), (Liao 2007) for extended review of these behaviors). Our complementary investigation from one individual shows that the configuration of SGM models can vary across behaviors; accelerating fish require more segments than steadily swimming fish, steady swimming fish require more segments than Kármán gaiting fish, and Kármán gaiting fish require more segments than gliding fish (supplementary figure 3). This behavior dependency poses a challenging question for robotics researchers: how to design a reconfigurable fish robot that is capable of changing its segment configuration automatically? Second, the SGM models are based on horizontal midline kinematics and do not consider three-dimensional body–fin and fin–fin interactions. Previous studies have shown that these interactions play key role to improve stability and propulsive efficiency (Liu *et al* 2017), (Matthews and Lauder 2021). Third, this study is only concerned with describing the midline kinematics accurately and identifying factors that may help us explain the variation we see in SGM models. However, it does not tell us why these variations exist in the first place nor how they relate to swimming performance and efficiency. For this, we need to better understand the mechanical and hydrodynamic forces controlling the kinematics. In this context, several theoretical models have been proposed to study fish swimming and guide robot designs (Epps *et al* 2009), (Tytell *et al* 2010), (Zhong *et al* 2018).

Future work will focus on analyzing how the segments of SGM models move with respect to each other and the earth frame of reference, as well as how these motions vary in relation to Re, morphology and swimming mode. We have also started building a modular fish robot which will allow us to explore different segment configurations (e.g. add more segments or increase the length of head segment) and evaluate the resulting swimming performance systematically.

Author contributions

OA conceived the research, developed the algorithms, analyzed the data and wrote the first draft of the manuscript. All authors contributed to data collection, interpretation of results and revision of the manuscript.

Acknowledgments

This research was supported by the Sér Cymru Cofund Research Fellowship (663830-AU167) and EU Staff Exchange Grant (H2020-MSCA-RISE-2019, 873178) to OA, the Office of Naval Research Grants (N000141410533 and N00014-15-1-2234) and NSF Grant (093088-17158) to GVL, Great Lakes Fisheries Commission Grant (2017-CAS-54063) to EG and TC-S, Fonds de Recherche Nature et Technologies du Québec to EG, National Oceanic and Atmospheric Administration Fisheries Grant (SER-2019-007) to TC-S, the National Science Foundation Grants (IOS1257150, IOS1856237), National Institute on Deafness and Other Communication Disorders Grant (RO1-DC-010809), Anonymous Foundation Grant, Patagonia Conservation Grant, and University of Florida Research Opportunity Seed Grant to JCL, NSF Grant (PRFB1907156) to DKW, and The Carl Tryggers Foundation Grant (20:98) to

VDS. The work was supported by the staff of each research facility involved in the project.

Data availability statement

The data that support the findings of this study are openly available at the following URL/DOI: https://doi.org/10.5061/dryad.bg79cnp9x.

ORCID iDs

Otar Akanyeti https://orcid.org/0000-0003-3515-6833
Valentina Di Santo https://orcid.org/0000-0002-5419-3747
Elsa Goerig https://orcid.org/0000-0003-1430-4657
Dylan K Wainwright https://orcid.org/0000-0003-4964-5048
James C Liao https://orcid.org/0000-0003-0181-6995
Theodore Castro-Santos https://orcid.org/0000-0003-2575-9120
George V Lauder https://orcid.org/0000-0003-0731-286X

References

Akanyeti O and Liao J C 2013a The effect of flow speed and body size on Kármán gait kinematics in rainbow trout *J. Exp. Biol.* **216** 3442–9

Akanyeti O and Liao J C 2013b A kinematic model of Kármán gaiting in rainbow trout *J. Exp. Biol.* **216** 4666–77

Akanyeti O, Putney J, Yanagitsuru Y R, Lauder G V, Stewart W J and Liao J C 2017 Accelerating fishes increase propulsive efficiency by modulating vortex ring geometry *Proc. Natl Acad. Sci. USA* **114** 13828–33

Akanyeti O, Thornycroft P J, Lauder G V, Yanagitsuru Y R, Peterson A N and Liao J C 2016 Fish optimize sensing and respiration during undulatory swimming *Nat. Commun.* **7** 11044

Altringham J D and Ellerby D J 1999 Fish swimming: patterns in muscle function *J. Exp. Biol.* **202** 3397–403

Anderson E J, Mcgillis W R and Grosenbaugh M A 2001 The boundary layer of swimming fish *J. Exp. Biol.* **204** 81–102

Anderson J, Streitlien K, Barrett D and Triantafyllou M 1998 Oscillating foils of high propulsive efficiency *J. Fluid Mech.* **360** 41–72

Ay M, Korkmaz D, Ozmen Koca G, Bal C, Akpolat Z and Bingol M 2018 Mechatronic design and manufacturing of the intelligent robotic fish for bio-inspired swimming modes *Electronics* **7** 118

Bainbridge R 1963 Caudal fin and body movement in the propulsion of some fish *J. Exp. Biol.* **40** 23–56

Blake R W 2004 Fish functional design and swimming performance *J. Fish. Biol.* **65** 1193–222

Borazjani I and Sotiropoulos F 2008 Numerical investigation of the hydrodynamics of carangiform swimming in the transitional and inertial flow regimes *J. Exp. Biol.* **211** 1541–58

Borazjani I and Sotiropoulos F 2009 Numerical investigation of the hydrodynamics of anguilliform swimming in the transitional and inertial flow regimes *J. Exp. Biol.* **212** 576–92

Breder C M Jr 1926 The locomotion of fishes *Zoologica* **4** 159–297

Carroll A M, Wainwright P C, Huskey S H, Collar D C and Turingan R G 2004 Morphology predicts suction feeding performance in centrarchid fishes *J. Exp. Biol.* **207** 3873–81

Castro-Santos T 2005 Optimal swim speeds for traversing velocity barriers: an analysis of volitional high-speed swimming behavior of migratory fishes *J. Exp. Biol.* **208** 421–32

Castro-Santos T, Cotel A and Webb P 2009 Fishway evaluations for better bioengineering: an integrative approach *Challenges for Diadromous Fishes in a Dynamic Global Environment* (Maryland: American Fisheries Society) p 557

Chambers L D, Akanyeti O, Venturelli R, Ježov J, Brown J, Kruusmaa M, Fiorini P and Megill W M 2014 A fish perspective: detecting flow features while moving using an artificial lateral line in steady and unsteady flow *J. R. Soc. Interface* **11** 20140467

Di Santo V, Goerig E, Wainwright D K, Akanyeti O, Liao J C, Castro-Santos T and Lauder G V 2021 Convergence of undulatory swimming kinematics across a diversity of fishes *Proc. Natl Acad. Sci. USA* **118** e2113206118

Domenici P and Blake R 1997 The kinematics and performance of fish fast-start swimming *J. Exp. Biol.* **200** 1165–78

El Daou H, Salumäe T, Chambers L D, Megill W M and Kruusmaa M 2014 Modelling of a biologically inspired robotic fish driven by compliant parts *Bioinsp. Biomim.* **9** 016010

Epps B P, Valdivia y Alvarado P, Youcef-Toumi K and Techet A H 2009 Swimming performance of a biomimetic compliant fish-like robot *Exp. Fluids* **47** 927–39

Fetherstonhaugh S E A W, Shen Q and Akanyeti O 2021 Automatic segmentation of fish midlines for optimizing robot design *Bioinsp. Biomim.* **16** 046005

Fish F E 1996 Transitions from drag-based to lift-based propulsion in mammalian swimming *Am. Zool.* **36** 628–41

Gazzola M, Argentina M and Mahadevan L 2014 Scaling macroscopic aquatic locomotion *Nat. Phys.* **10** 758–61

Gemmell B J, Fogerson S M, Costello J H, Morgan J R, Dabiri J O and Colin S P 2016 How the bending kinematics of swimming lampreys build negative pressure fields for suction thrust *J. Exp. Biol.* **219** 3884–95

Gillis G 1997 Anguilliform locomotion in an elongate salamander (*Siren intermedia*): effects of speed on axial undulatory movements *J. Exp. Biol.* **200** 767–84

Goerig E, Di Santo V, Wainwright D K, Castro-Santos T, Liao J C, Akanyeti O and Lauder G V 2021 Convergence of undulatory swimming kinematics across a diversity of fishes *Dryad Dataset*

Gray J 1933 Directional control of fish movement *Proc. R. Soc.* B **113** 115–25

Jayne B C and Lauder G V 1995 Speed effects on midline kinematics during steady undulatory swimming of largemouth bass, *Micropterus salmoides J. Exp. Biol.* **198** 585–602

Jusufi A, Vogt D M, Wood R J and Lauder G V 2017 Undulatory swimming performance and body stiffness modulation in a soft robotic fish-inspired physical model *Soft Robot.* **4** 202–10

Karakasiliotis K, Thandiackal R, Melo K, Horvat T, Mahabadi N K, Tsitkov S, Cabelguen J M and Ijspeert A J 2016 From cineradiography to biorobots: an approach for designing robots to emulate and study animal locomotion *J. R. Soc. Interface* **13** 20151089

Katzschmann R K, Delpreto J, Maccurdy R and Rus D 2018 Exploration of underwater life with an acoustically controlled soft robotic fish *Sci. Robot.* **3** eaar3449

Kruusmaa M *et al* 2014 FILOSE for svenning: a flow sensing bioinspired robot *IEEE Robot. Autom. Mag.* **21** 51–62

Langerhans R B 2009 Trade-off between steady and unsteady swimming underlies predator-driven divergence in *Gambusia affinis J. Evol. Biol.* **22** 1057–75

Lauder G V 2000 Function of the caudal fin during locomotion in fishes: kinematics, flow visualization, and evolutionary patterns *Am. Zool.* **40** 101–22

Lauder G V and Tytell E D 2005 Hydrodynamics of undulatory propulsion *Fish Physiol.* **23** 425–68

Li G, Liu H, Müller U K, Voesenek C J and van Leeuwen J L 2021 Fishes regulate tail-beat kinematics to minimize speed-specific cost of transport *Proc. R. Soc.* B **288** 20211601

Liao J C 2007 A review of fish swimming mechanics and behaviour in altered flows *Phil. Trans. R. Soc.* B **362** 1973–93

Lighthill M J 1969 Hydromechanics of aquatic animal propulsion *Annu. Rev. Fluid Mech.* **1** 413–46

Lighthill S J 1993 Estimates of pressure differences across the head of a swimming clupeid fish *Proc. R. Soc.* B **341** 129–40

Lindsey C 1978 Form, function and locomotory habits in fish *Locomotion* (New York: Academic Press)

Liu G, Ren Y, Dong H, Akanyeti O, Liao J C and Lauder G V 2017 Computational analysis of vortex dynamics and performance enhancement due to body–fin and fin–fin interactions in fish-like locomotion *J. Fluid Mech.* **829** 65–88

Liu J and Hu H 2010 Biological inspiration: from carangiform fish to multi-joint robotic fish *J. Bionic Eng.* **7** 35–48

Liu J-D and Hu H 2006 Biologically inspired behaviour design for autonomous robotic fish *Int. J. Autom. Comput.* **3** 336–47

Long J, Hale M, Mchenry M and Westneat M 1996 Functions of fish skin: flexural stiffness and steady swimming of longnose gar, *Lepisosteus osseus J. Exp. Biol.* **199** 2139–51

Long J H Jr and Nipper K S 1996 The importance of body stiffness in undulatory propulsion *Am. Zool.* **36** 678–94

Low K H and Chong C W 2010 Parametric study of the swimming performance of a fish robot propelled by a flexible caudal fin *Bioinsp. Biomim.* **5** 046002

Lucas K N, Lauder G V and Tytell E D 2020 Airfoil-like mechanics generate thrust on the anterior body of swimming fishes *Proc. Natl Acad. Sci. USA* **117** 10585–92

Marchese A D, Onal C D and Rus D 2014 Autonomous soft robotic fish capable of escape maneuvers using fluidic elastomer actuators *Soft Robot.* **1** 75–87

Matthews D and Lauder G V 2021 Fin–fin interactions during locomotion in a simplified biomimetic fish model *Bioinsp. Biomim.* **16** 046023

Mu¨ller U K and van Leeuwen J L 2004 Swimming of larval zebrafish: ontogeny of body waves and implications for locomotory development *J. Exp. Biol.* **207** 853–68

Nangia N, Bale R, Chen N, Hanna Y and Patankar N A 2017 Optimal specific wavelength for maximum thrust production in undulatory propulsion *PLoS One* **12** e0179727

Ozmen Koca G, Bal C, Korkmaz D, Bingol M, Ay M, Akpolat Z and Yetkin S 2018 Three-dimensional modeling of a robotic fish based on real carp locomotion *Appl. Sci.* **8** 180

Raj A and Thakur A 2016 Fish-inspired robots: design, sensing, actuation, and autonomy—a review of research *Bioinsp. Biomim.* **11** 031001

Rossi C, Colorado J, Coral W and Barrientos A 2011 Bending continuous structures with SMAs: a novel robotic fish design *Bioinsp. Biomim.* **6** 045005

Rouleau S, Glémet H and Magnan P 2010 Effects of morphology on swimming performance in wild and laboratory crosses of brook trout ecotypes *Funct. Ecol.* **24** 310–21

Sfakiotakis M, Lane D M and Davies J B C 1999 Review of fish swimming modes for aquatic locomotion *IEEE J. Ocean. Eng.* **24** 237–52

Shadwick R E and Lauder G V 2006 *Fish Physiology: Fish Biomechanics* (Amsterdam: Elsevier)

Smits A J 2019 Undulatory and oscillatory swimming *J. Fluid Mech.* **874** P1

Su Z, Yu J, Tan M and Zhang J 2014 Implementing flexible and fast turning maneuvers of a multijoint robotic fish *IEEE/ASME Trans. Mechatronics* **19** 329–38

Tan J, Tan H, Goerig E, Ke S, Huang H, Liu Z and Shi X 2021 Optimization of fishway attraction flow based on endemic fish swimming performance and hydraulics *Ecol. Eng.* **170** 106332

Taylor G K, Nudds R L and Thomas A L R 2003 Flying and swimming animals cruise at a Strouhal number tuned for high power efficiency *Nature* **425** 707–11

Thandiackal R *et al* 2021 Emergence of robust self-organized undulatory swimming based on local hydrodynamic force sensing *Sci. Robot.* **6** eabf6354

Tytell E D 2010 Do trout swim better than eels? Challenges for estimating performance based on the wake of self-propelled bodies *Animal Locomotion* (Berlin: Springer)

Tytell E D, Hsu C-Y, Williams T L, Cohen A H and Fauci L J 2010 Interactions between internal forces, body stiffness, and fluid environment in a neuromechanical model of lamprey swimming *Proc. Natl Acad. Sci. USA* **107** 19832–7

Tytell E D and Lauder G V 2004 The hydrodynamics of eel swimming: I. Wake structure *J. Exp. Biol.* **207** 1825–41

Tytell E D, Leftwich M C, Hsu C-Y, Griffith B E, Cohen A H, Smits A J, Hamlet C and Fauci L J 2016 Role of body stiffness in undulatory swimming: insights from robotic and computational models *Phys. Rev. Fluids* **1** 073202

Valdivia y Alvarado P and Youcef-Toumi K 2006 Design of machines with compliant bodies for biomimetic locomotion in liquid environments *J. Dyn. Syst. Meas. Control* **128** 3–13

Van Buren T, Floryan D and Smits A J 2019 Scaling and performance of simultaneously heaving and pitching foils *AIAA J.* **57** 3666–77

Van Rees W M, Gazzola M and Koumoutsakos P 2015 Optimal morphokinematics for undulatory swimmers at intermediate Reynolds numbers *J. Fluid Mech.* **775** 178–88

Venturelli R *et al* 2012 Hydrodynamic pressure sensing with an artificial lateral line in steady and unsteady flows *Bioinsp. Biomim.* **7** 036004

Wardle C, Videler J and Altringham J 1995 Tuning in to fish swimming waves: body form, swimming mode and muscle function *J. Exp. Biol.* **198** 1629–36

Webb P W 1982 Locomotor patterns in the evolution of actinopterygian fishes *Am. Zool.* **22** 329–42

Webb P W 1984 Body form, locomotion and foraging in aquatic vertebrates *Am. Zool.* **24** 107–20

Webb P W, Kostecki P T and Stevens E D 1984 The effect of size and swimming speed on locomotor kinematics of rainbow trout *J. Exp. Biol.* **109** 77–95

White C, Lauder G V and Bart-Smith H 2021 Tunabot Flex: a tuna-inspired robot with body flexibility improves high-performance swimming *Bioinsp. Biomim.* **16** 026019

Yanagitsuru Y R, Akanyeti O and Liao J C 2018 Head width influences flow sensing by the lateral line canal system in fishes *J. Exp. Biol.* **221**

Yu J, Wang L and Tan M 2007 Geometric optimization of relative link lengths for biomimetic robotic fish *IEEE Trans. Robot.* **23** 382–6

Zhong Y, Li Z and Du R 2017 A novel robot fish with wire-driven active body and compliant tail *IEEE/ASME Trans. Mechatronics* **22** 1633–43

Zhong Y, Song J, Yu H and Du R 2018 Toward a transform method from lighthill fish swimming model to biomimetic robot fish *IEEE Robot. Autom. Lett.* **3** 2632–9